JOURNAL OF THEORETICAL
AND APPLIED MECHANICS
https://doi.org/10.15632/jtam-pl/199928
ONLINE FIRST

PERFORMANCE BENEFITS OF VEHICLE AIR SUSPENSION SYSTEM EMPLOYING INERTER ELEMENT

Yujie SHEN*, Jiaheng LIN, Yuqiu XU, Xiaofeng YANG, Yanling LIU

Automotive Engineering Research Institute, Jiangsu University, Zhenjiang 212013, China
*corresponding author, *shenyujie@ujs.edu.cn*

This paper analyzes the performance analysis of vehicle air inerter-spring-damper (ISD) suspension systems. First of all, this paper establishes the air ISD suspension with series-connected inerter and with parallel-connected inerter which are the quarter car model of the two basic vehicle suspension layouts involving an inerter. After that, the primary parameters are optimized through particle swarm optimization by considering the overall performance, including vehicle body acceleration, suspension working space and dynamic tire load. The simulation analysis reveals that all of the dynamic performance indexes of the vehicle air ISD suspension are significantly decreased by comparing to the conventional air suspension. A bench test was carried out to verify that the model assumptions and simplifications are correctly formulated.

Keywords: inerter; vehicle suspension; air suspension; ride comfort.

Articles in JTAM are published under Creative Commons Attribution 4.0 International.
Unported License https://creativecommons.org/licenses/by/4.0/deed.en.
By submitting an article for publication, the authors consent to the grant of the said license.

1. Introduction

The vehicle suspension, a general device situated between the wheel and the axle for the force transmission, which can maintain the vehicle ride comfort and ensuring handling stability. So far, the semi-active suspension (Elahi *et al.*, 2016; Sammier *et al.*, 2003) and active suspension (Cui *et al.*, 2019; Li *et al.*, 2023) systems can be self-adjusted according to changes in driving conditions. Different from the general suspension, the air suspension (Oda & Nishimura, 1970; Quaglia & Sorli, 2001; Shen *et al.*, 2024b) replaces the plate spring in the traditional suspension with the air spring. Due to the nonlinear characteristics of the airbag (Wen *et al.*, 2013), the variable stiffness characteristics of the air spring can be guaranteed, which can improve the ride comfort while ensuring the vehicle handling stability. Li *et al.* (2014) creates the model of interlinked air suspension, confirming that the vehicle's roll angle and vertical vibration will be reduced effectively by using the proposed suspension. However, the air suspension still maintains the "spring-damper" structure of the traditional suspension system, which is still limited in improving the performance of the suspension. With the development of suspension technology, active suspension (Yang *et al.*, 2024) and semi-active suspension (Shen *et al.*, 2024a) has been studied widely. But from the view of energy consumption and reliability, semi-active suspension and active suspension still have a long way to engineering application. From this perspective, it is more reasonable to enhance the suspension performance by using a passive element.

Smith (2002) from Cambridge University first proposed the concept of interter. It represents a departure from the common structure of the traditional suspension "spring-damper". The force applied at both ends of the mechanical element is proportional to the relative accelerations. The application of the inerter to the vehicle suspension, that is, the "inerter-spring-damper" structure (ISD suspension), has pushed the development of the vehicle suspension system to a new platform (Shen *et al.*, 2023a; 2023b; Wang *et al.*, 2024a; 2024b). To date, dif-

ferent realizations of inerter have been developed, including ball-screw inerter (Ma *et al.*, 2021), rack-and-pinion inerter (Papageorgiou *et al.*, 2009), hydraulic inerter (Wang *et al.*, 2011), electromagnetic mechanism inerter (Gonzalez-Buelga *et al.*, 2015), helical fluid inerter (De Domenico *et al.*, 2019) and living-hinge inerter (John & Wagg, 2019). Seifi and Hassannejad (2022) introduces a novel suspension design featuring inerters and asymmetric dampers, and it is confirmed that the ride comfort and road-holding ability can be improved by using the optimized suspension with inerters and nonlinear dampers.

Currently, there is limited research by scholars on the integration of inerters into suspension systems to improve the air suspension performance. The air suspension of the existing research still maintains the "spring-damper" structure of the traditional suspension system, and the performance of the air suspension with inerter is unknown. In this paper, on the basis of the air suspension, the inerter will be included and the performance of the air ISD suspension will be explored.

The structure of the paper is organized in the following manner: in Section 2, a new air ISD suspension structure is introduced, along with the establishment of the models for air ISD suspension that including both series-connected and parallel-connected inerter. Section 3 employs the particle swarm optimization algorithm to complete the optimization under random road input conditions. In Section 4, the two suspension models will be simulated and analyzed in both the time and frequency domains under various road conditions. In Section 5, the bench test was carried out to verify that the model assumptions and simplifications are correctly formulated in the paper. The paper concludes with a summary in Section 6.

2. Model of the vehicle air ISD suspension

An accurate model that takes into account various connectivity relationships and nonlinear factors is essential for accurately capturing the dynamic response of real vehicles. There are many studies on vehicle suspension performance using a 7 degree-of-freedom (dof) model and even a 14 dof model. However, an accurate model is often too complicated, and there have been studies using a 2 dof model to demonstrate vehicle suspension performance (Shen *et al.*, 2023b). This paper focuses on the general laws of the inerter's benefits on the vehicle vertical dynamics performance. Consequently, this paper considers the nonlinear stiffness feature of the air spring and establishes a 2 dof quarter car ISD suspension model. Among this dynamic model, the car body and wheel are assumed to be rigid bodies with concentrated mass. The inerter, air spring and damper are connected according to series arrangement and parallel arrangement between the sprung mass and unsprung mass. The effect of tire damping is neglected, and the tires are simplified as equivalent springs connected to the road surface. The conventional air suspension model is marked as S_0 and the series-connected air suspension and parallel-connected air suspension are marked as S_1 and S_2, respectively, as shown in Fig. 1.

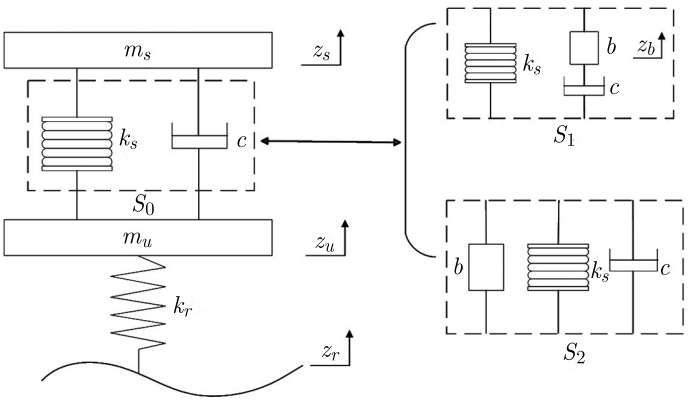

Fig. 1. Vehicle air ISD suspension.

Here, m_s represents the mass of the sprung component, m_u denotes the mass of the unsprung component, k_r represents the stiffness of tire, z_s, z_u, and z_r denotes the vertical displacements of the sprung mass, unsprung mass and road input, respectively.

For a sleeve model air spring with a negligible change in effective area and hysteresis effect, the stiffness of the air spring is formulated as follows:

$$k_s = \frac{np_0}{v_0 - A_e(z_u - z_s)} A_e^2, \tag{2.1}$$

where p_0 represents the initial effective air pressure, v_0 represents the initial volume, A_e represents the effective area and n represents the thermos dynamic coefficient.

There are many realization forms of inerters and different types of inerters have a different mathematical model. But the ideal inerter output force is related with the acceleration between two terminals. Consider the length of this paper, the ideal inerter output force can be summarized as follow:

$$F_b = b\ddot{x}, \tag{2.2}$$

where b represents the inertance with the unit kg, $\ddot{x}$ is the acceleration between two terminals.

The suspension has two basic arrangements, namely series arrangement and parallel arrangement. In this document, the inerter structure is added on the basis of air suspension, and two new structural forms of suspension are constructed, called series-connected air suspension and parallel-connected air suspension with the inerter component, as demonstrated in parts S_1 and S_2 of Fig. 1.

Where b represents the inertance with the unit kg, z_b represents the vertical displacement of the inerter, pertaining to the sprung mass denoted as m_s, based on Newton's laws of motion, the equation is described as follows:

$$m_s\ddot{z}_s + b(\ddot{z}_s - \ddot{z}_b) + k_s(z_s - z_u) = 0. \tag{2.3}$$

For the unsprung mass denoted as m_u, the equation is described as follows:

$$m_u\ddot{z}_u - k_s(z_s - z_u) - c(\dot{z}_b - \dot{z}_u) + k_r(z_u - z_r) = 0. \tag{2.4}$$

At the connection point of the inerter to the damping mechanism, the equation is described as follows:

$$b(\ddot{z}_s - \ddot{z}_b) = c(\dot{z}_b - \dot{z}_u). \tag{2.5}$$

After that, the equations describing the motion of the entire system are as follows:

$$\begin{aligned} m_s\ddot{z}_s + b(\ddot{z}_s - \ddot{z}_b) + k_s(z_s - z_u) &= 0, \\ m_u\ddot{z}_u - k_s(z_s - z_u) - c(\dot{z}_b - \dot{z}_u) + k_r(z_u - z_r) &= 0, \\ b(\ddot{z}_s - \ddot{z}_b) &= c(\dot{z}_b - \dot{z}_u). \end{aligned} \tag{2.6}$$

The S_2 part of Fig. 1 illustrates a quarter car model incorporating an inerter. The inerter is connected in parallel with the damping element in this model. It is intuitively to figure out the motion equation of this system according to the above analysis of the series-connected system.

For the sprung mass denoted as m_s, based on Newton's laws of motion, the equation is described as follows:

$$m_s\ddot{z}_s + b(\ddot{z}_s - \ddot{z}_u) + k_s(z_s - z_u) + c(\dot{z}_s - \dot{z}_u) = 0. \tag{2.7}$$

For the unsprung mass denoted as m_u, the equation is described as follows:

$$m_u\ddot{z}_u - b(\ddot{z}_s - \ddot{z}_u) - k_s(z_s - z_u) - c(\dot{z}_s - \dot{z}_u) + k_r(z_u - z_r) = 0. \tag{2.8}$$

After that, the equations describing the motion of the entire system are as follows:

$$\begin{aligned} m_s\ddot{z}_s + b(\ddot{z}_s - \ddot{z}_u) + k_s(z_s - z_u) + c(\dot{z}_s - \dot{z}_u) &= 0, \\ m_u\ddot{z}_u - b(\ddot{z}_s - \ddot{z}_u) - k_s(z_s - z_u) - c(\dot{z}_s - \dot{z}_u) + k_r(z_u - z_r) &= 0. \end{aligned} \tag{2.9}$$

3. Optimization of the suspension parameters

In the optimization process, the root-mean-square (RMS) values of vehicle body acceleration, suspension working space, and dynamic tire load incorporates the consideration so that the vehicle air ISD suspension can get optimized. It is assumed that the vehicle drives with a speed of v on a Grade C road, with the random road input being characterized as follows:

$$\dot{z}_r(t) = -0.111\left[vz_r(t) + 40\sqrt{G_q(n_0)v}\omega(t)\right], \tag{3.1}$$

where the vertical displacement of the random road input can be expressed as $z_r(t)$, the road roughness can be expressed as $G_q(n_0)$, and the Gaussian white noise with mean value as 0 can be expressed as $\omega(t)$. Here, $G_q(n_0)$ is $256 \times 10^{-6}\,\mathrm{m}^3 \cdot \mathrm{cycle}^{-1}$, v is 20 m/s. Particle swarm optimization (PSO) is a swarm intelligence algorithm, which regards the behavior of optimizing the objective function as the cooperation and competition among individuals in the predatory behavior of birds. During the simulation optimization in this paper, the PSO is adopted.

3.1. Parameters optimization of S_1 and S_2

When using the PSO to determine the optimal parameters of S_1 and S_2, the damping coefficient and the inertance are variables and require optimization, and the rest of the suspension model parameters are provided in Table 1.

Table 1. Parameters of the mature air suspension model.

Parameter name	Value
Sprung mass, m_s	800 kg
Unsprung mass, m_u	100 kg
Stiffness of tire, k_r	243000 N/m
Passive damping coefficient, c_0	2000 Ns/m
Air spring initial air pressure, p_0	188000 Pa
Initial volume of air spring, v_0	0.0116 m^3
Effective area of air spring, A_e	0.0421 m^2
Air polytropic index, n	1

Using S_0 as the comparison object, the optimization objectives include the RMS of the vehicle body acceleration, the suspension working space and the dynamic tire load. A unified objective function is then formulated, and MATLAB/Simulink is employed to determine the optimal solution of this objective function along with its specific parameters.

It should be noted that, under random road inputs, the RMS values for the vehicle body acceleration, the suspension working space, and the dynamic tire load of S_0 are 0.4828 $\mathrm{m/s}^2$, 0.0072 m, 625.16 N, respectively. Establishing a unified objective function is essential, given that the above three performance indexes differ in units and magnitudes. To examine the overall dynamic performances, encompassing ride comfort, handling stability, and driving safety, of the proposed vehicle air ISD suspension, a comprehensive objective is formulated. Divide the three indexes of the suspension with S_1 and the three indexes of S_0 separately, then the unified objective function is the sum of three quotients. The formula for the unified objective function is as follows:

$$f = 0.6 \times J_1/J_{1\mathrm{pas}} + 0.2 \times J_2/J_{2\mathrm{pas}} + 0.2 \times J_3/J_{3\mathrm{pas}}, \tag{3.2}$$

where the fitness function can be expressed as f, J_1, J_2, J_3, respectively, represent the RMS of the body acceleration, the suspension working space and the dynamic tire load of the vehicle air

ISD suspension, while $J_{1\text{pas}}$, $J_{2\text{pas}}$, and $J_{3\text{pas}}$ are the RMS values of the vehicle body acceleration, the suspension working space and the dynamic tire load of S_0, respectively. The penalty rule is established such that, among the RMS values of body acceleration, suspension working space, and dynamic tire load, if any one of these is inferior to the corresponding value of S_0, the penalty value is assigned as 100; otherwise, it is set to 0. Represents the upper and lower limits of parameters to be optimized can be expressed as lb and ub, respectively, given that the actual structure, $lb = [1, 1]$, $ub = [2000, 5000]$.

When the maximum number of iterations is 30, the group size is 10, the inertia coefficient is 0.8, the damping ratio of the inertia coefficient is 0.9, the individual acceleration coefficient c_1 is 1.5, the social acceleration coefficient c_2 is 2. The optimal parameters for S_1 and S_2 are detailed in Table 2.

Table 2. Optimization results of S_1 and S_2.

Suspension	Inertance b [kg]	Damping coefficient c [Ns/m]
S_1	793	3362
S_2	17	3190

4. Dynamic performance analysis

After using the optimized parameters in Section 3, time domain and frequency domain simulations for S_1 and S_2 under various working conditions are conducted so that the improvement of the performance of the air suspension by the inerter can get deeper research.

4.1. Simulation under the random road

Figures 2–4 show the three dynamic performance indexes of S_1 and S_2 compared to S_0 on the random road surface at a speed of 20 m/s, where (a) is the time domain response and (b) is the frequency domain response.

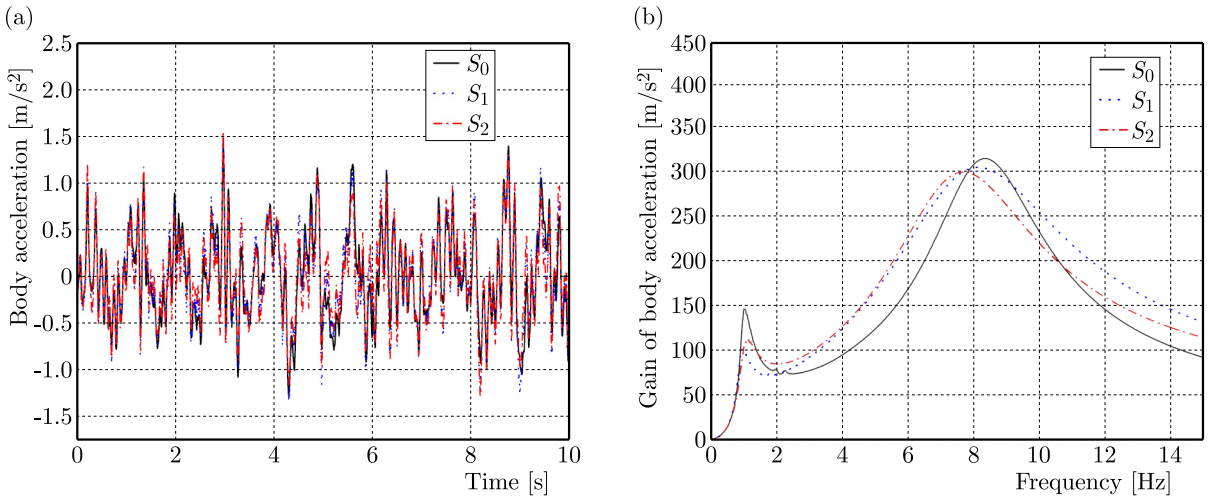

Fig. 2. Responses of vehicle body acceleration under the random road.

Table 3 shows the dynamic performance indexes of S_0, S_1, and S_2 on the random road surface at a speed of 20 m/s.

In the frequency domain responses, as the frequency increases, all the gain value of the three indexes increases first and then decreases in the low frequency band, and have a trend of increas-

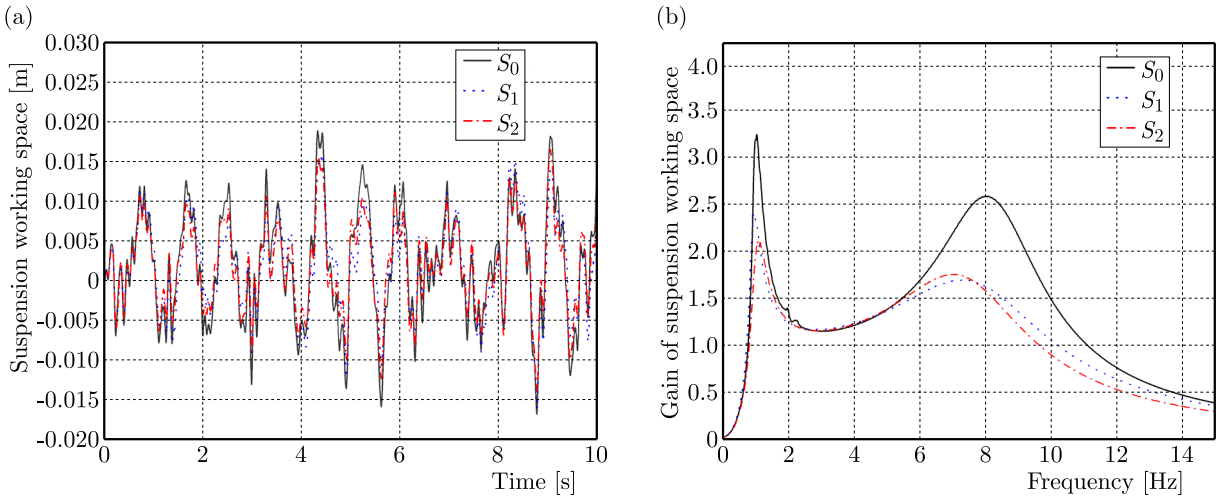

Fig. 3. Responses of suspension working space under the random road.

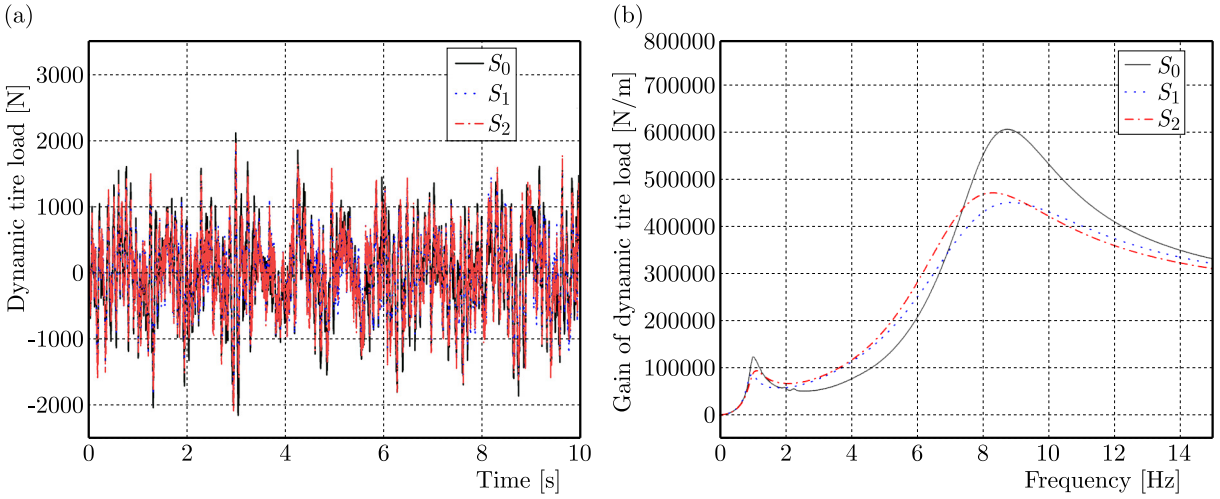

Fig. 4. Responses of dynamic tire load under the random road.

Table 3. Dynamic performance indexes.

Indexes	S_0	S_1	S_2
RMS of body acceleration [m/s^2]	0.48	0.45	0.47
RMS of suspension working space [m]	0.0072	0.0060	0.0058
RMS of dynamic tire load [N]	625	556	589

ing before decreasing in the high frequency band, with each frequency band displaying a peak value. From Fig. 4, for the vehicle body acceleration, the peak of S_1 in the low frequency is obviously lower than S_0, which decreases from 148.4 to 101.7 [(m/s^2)/m], compared with S_2 from 148.4 to 113.9, it has a great improvement of 31.4 %. But for the high frequency peak, the change of both S_1 and S_2 is small, S_1 decreases by 3.6 %, and S_2 decreases by 2.4 %. The performance improvement of the suspension workspace is greater compared to the acceleration of the vehicle body. The low frequency peak of S_1 is reduced from 3.2 to 2.5 (marking a reduction of 21.8 %), the peak of S_2 from 3.3 to 2.1 (marking a reduction of 36.4 %), the high frequency peak of S_1 is reduced from 2.6 to 1.6 (marking a reduction of 38.5 %), and the high frequency peak of S_2 is reduced from 2.6 to 1.8 (marking a reduction of 30.1 %). For the dynamic tire load analysis, the low frequency peak of S_1 is reduced from 124228 to 85080 (marking a reduction of

31.5 %), the peak of S_2 is reduced from 124228 to 95040 (marking a reduction of 23.5 %), the high frequency peak of S_1 is reduced from 610471 to 436081 (marking a reduction of 28.6 %), and the high frequency peak of S_2 is reduced from 610471 to 474744 (marking a reduction of 22.2 %). As can be observed from the above figures and tables that, both of the dynamic performance of S_1 and S_2 are improved compared with S_0. For the time domain, the body acceleration and the dynamic tire load of S_1 are better than S_2, and S_2 is better than S_1 regarding the dynamic performance of the suspension working space. While for the frequency domain, both S_1 and S_2 can make the suspension obtain enhanced dynamic performance, handling stability ride and comfort.

4.2. Time domain analysis under pulse road input

According to the GB5902-86, it is assumed that the vehicle passes through the long-wave soil block at a speed of 10 m/s, which is used as the input of the pulse-type excitation displacement. As the road input is different, if the inertance and the damping coefficient optimized by the random road surface are brought into the pulse road input, there will be a number of dynamic performance deterioration. As a consequence, S_1 and S_2 under the pulse road input are re-optimized using the particle swarm optimization algorithm. For S_1, the optimized inertance coefficient is 485.6 kg, and the damping coefficient is 2238.6 Ns/m. For S_2, the optimized inertance coefficient is 14.9 kg, and the damping coefficient is 1087.9 Ns/m. Figure 5 shows three dynamic performance indexes of S_1 and S_2 compared with S_0 under a pulse input in the time-domain.

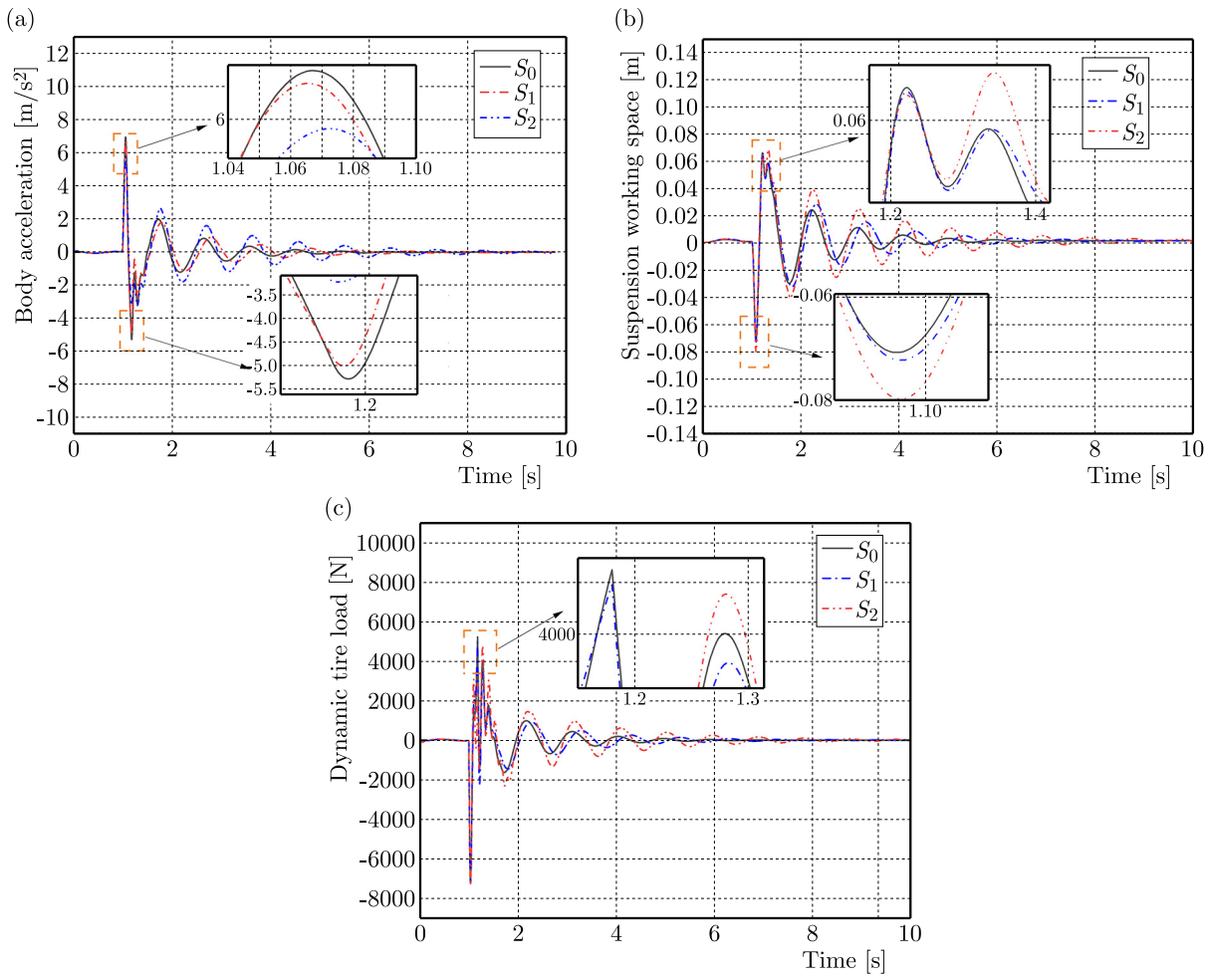

Fig. 5. Dynamic performance indexes under pulsed road.

Table 4 shows the dynamic performance indexes of S_1 and S_2 under a pulse input. The figures and tables clearly show that, compared with S_0, the peak-to-peak (PTP) value of vehicle body acceleration of S1 decreased by 4.1 %, and the PTP value of dynamic tire load decreased by 1.9 %, while the PTP value of body acceleration of S_2 decreased by 26.2 %, and the PTP value of dynamic tire load decreased by 2.5 %. On the contrary, for the suspension working space, S_1 and S_2 are increased slightly. In order to find out the reason, the three-dimensional diagram of S_1 and S_2 is shown. The inertance coefficient is the X-axis, the damping coefficient is the Y-axis, and the PTP values of the three dynamic performances are the Z-axis, so that the PTP values of the three dynamic performances can be clearly observed with the inertance coefficient and damping coefficient.

Table 4. Dynamic performance indexes under pulse input.

Name	S_0	S_1	S_2
PTP of vehicle body acceleration [m/s^2]	12.2	11.7	9.0
PTP of dynamic tire load [N]	12381	12149	12067
PTP of suspension working space [m]	0.1366	0.1373	0.1483

Figures 6–8 show the variation trend of PTP value of the body acceleration, suspension working space and dynamic tire load of S_1 and S_2 with damping coefficient and inertance

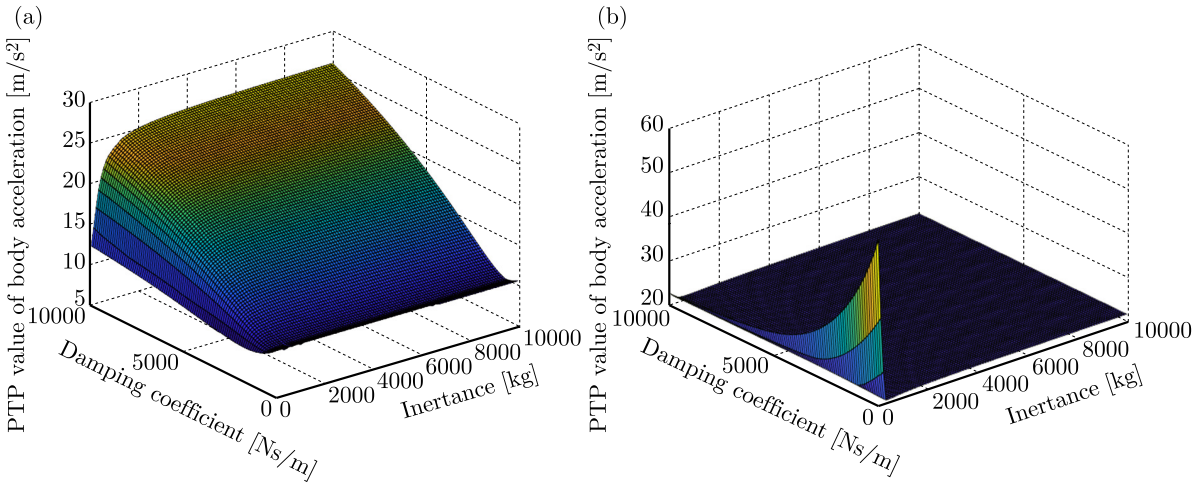

Fig. 6. Change trend of body acceleration under pulse road surface.

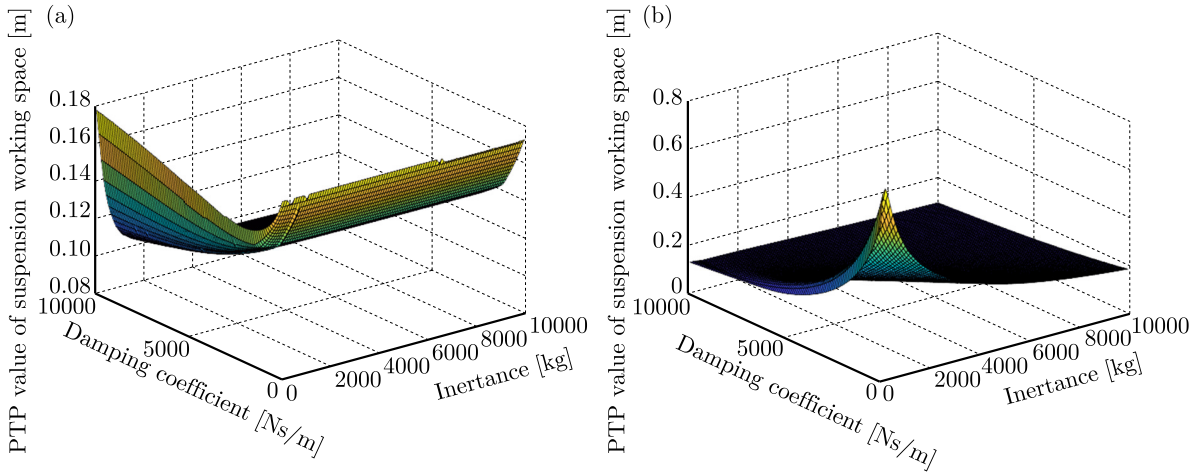

Fig. 7. Change trend of suspension working space under pulse road surface.

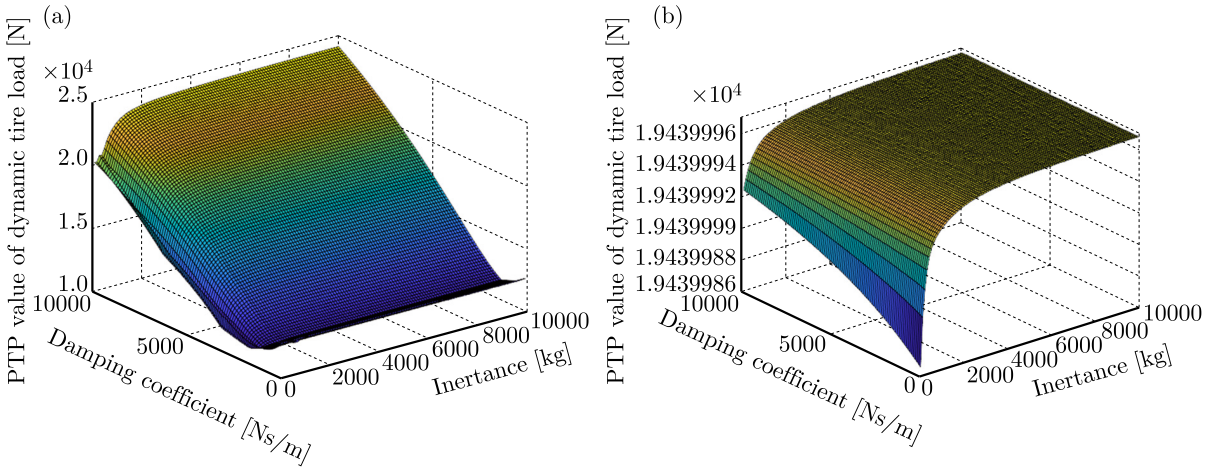

Fig. 8. Change trend of dynamic tire load under pulse road surface.

coefficient compared with the traditional air suspension under a pulse input, where (a) is S_1 and (b) is S_2.

As shown in the above figure, for the S_1, the PTP trend of the dynamic tire load and the body acceleration is basically the same, but the suspension working space is different. Therefore, in the optimization process of this paper, the weight coefficients of body acceleration and dynamic tire load in the fitness function are set to 0.4, and the weight coefficient of suspension working space is set to 0.2, so as to achieve the best overall optimization effect. However, it is obvious that according to the three-dimensional diagram, when the PTP value of body acceleration and dynamic tire load is minimized, the PTP value of suspension working space shows an upward trend. Compared with the traditional air suspension, the dynamic performance of suspension working space is deteriorated, and the expected optimization effect cannot be achieved at the same time. In the S_2 as shown in the figure, the three dynamic performance trends with the inertance coefficient and the damping coefficient are not the same, and the optimal points of the three dynamic performance cannot be achieved in the same place. Therefore, in the process of optimization in this paper, when the PTP value of body acceleration is minimized, the PTP values of dynamic tire load and the suspension working space are not at the lowest point. The PTP value of dynamic tire load is slightly improved compared with the traditional air suspension, while the dynamic performance of suspension workspace is deteriorated.

5. Experimental research

To verify the performance benefits of a vehicle air suspension system employing an inerter, a bench test was carried out to demonstrate the results obtained in Section 4. The overall layout of the bench test is shown in Fig. 9. The suspension parameters are the same as in Table 1 and Table 2. A fluid inerter which can create the damping effect and inertia effect simultaneously was used in this experiment. The suspension structures S_1 and S_2 can achieve by changing the parts inside the fluid inerter as shown in Figs. 9a and 9b.

Taking the C-level random road simulated in Section 4 as the test road input. The test result is shown in Fig. 10 and Table 5.

Table 5. Comparison of RMS of vehicle body acceleration in bench test.

Indexes	S_0	S_1	S_2
RMS of body acceleration [m/s^2]	0.55	0.52	0.54

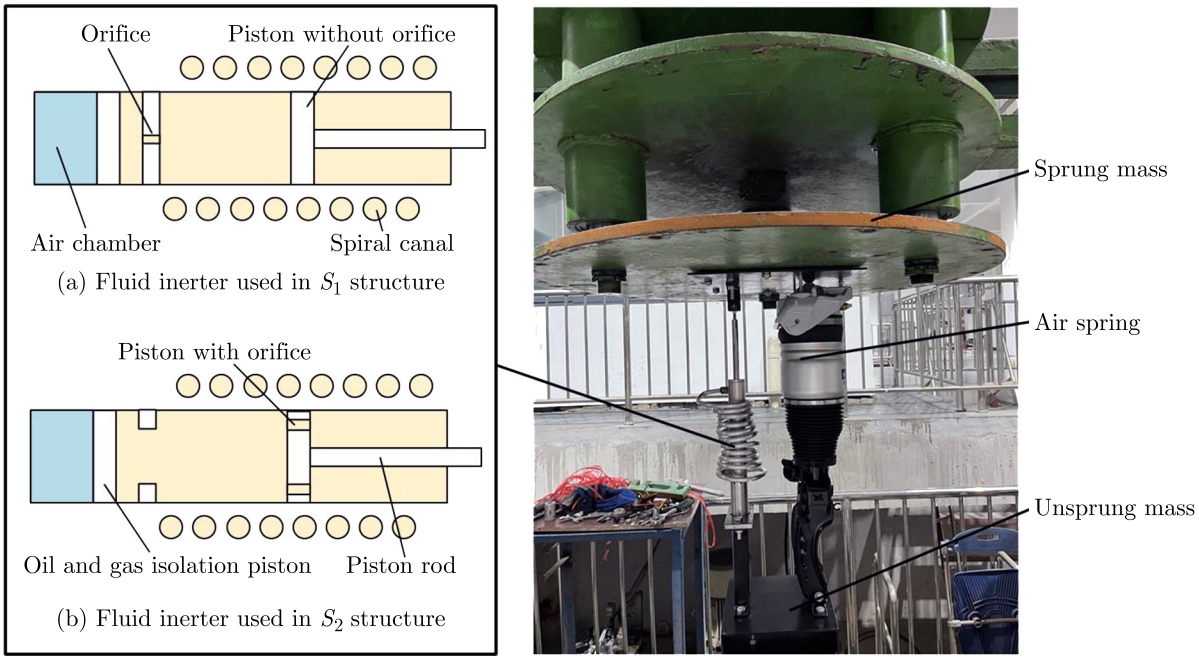

Fig. 9. Overall layout of bench test.

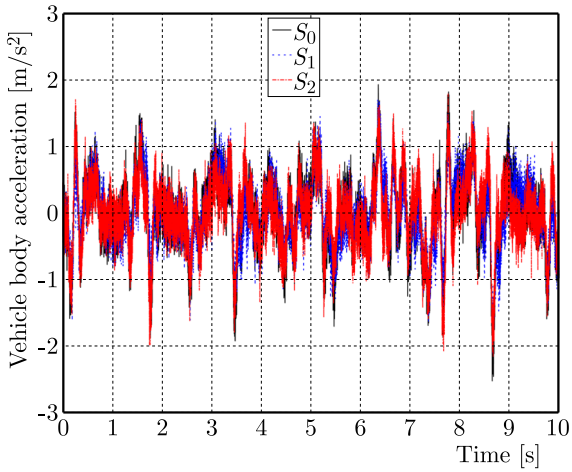

Fig. 10. Test comparison diagram of random road input.

Compared with the S_0 suspension, the RMS value of the body acceleration of the S_1 suspension reduced by 5.5 %, the RMS value of body acceleration of S_2 reduced by 1.8 %. There are some differences between the experimental data and the simulation results, which are initially analysed to be due to the sensor noise interference and system nonlinear factors. However, from the comparison of experimental results, the vibration suppression performances of the S_1 suspension superior to the S_0 suspension and S_2 suspension, which is consistent with the theoretical simulation.

6. Conclusion

This paper researches the performance benefits of the vehicle air suspension system using an inerter. Through designing the quarter car models of the two basic vehicle ISD suspension, the series-connected suspension and the parallel-connected suspension are created. Considering the overall suspension performance, key parameters of the two suspension systems are op-

timized through the PSO. In the time domain and the frequency domain a simulation analysis of the two suspension models was carried out, the findings indicate that, the dynamic performance of the suspension working space, dynamic tire load and body acceleration of the air ISD suspension with an inerter is enhanced, which confirms that the air ISD suspension can enhance the comfortable vehicle ride and the performance of road handling. The bench test was carried out and verified that the model assumptions and simplifications are correctly formulated in the paper.

Acknowledgments

This work was supported by National Natural Science Foundation of China (grant no. 52072157), China Postdoctoral Science Foundation (no. 2024T171048, 2024M753653), Young Elite Scientists Sponsorship Program by CAST (grant no. 2022QNRC001), Qing Lan Project of Jiangsu Province, China.

References

1. Cui, L.F., Xue, X.Y., Le, F.X., Mao, H.P., & Ding, S.M. (2019). Design and experiment of electro hydraulic active suspension for controlling the rolling motion of spray boom. *International Journal of Agricultural and Biological Engineering*, *12*(4), 72–81. https://doi.org/10.25165/j.ijabe.20191204.4648
2. De Domenico, D., Deastra, P., Ricciardi, G., Sims, N.D., & Wagg, D.J. (2019). Novel fluid inerter based tuned mass dampers for optimised structural control of base-isolated buildings. *Journal of the Franklin Institute*, *356*(14), 7626–7649. https://doi.org/10.1016/j.jfranklin.2018.11.012
3. Elahi, H., Israr, A., Khan, M.Z., & Ahmad, S. (2016). Robust vehicle suspension system by converting active & passive control of a vehicle to semi-active control system analytically. *Journal of Automation and Control Engineering*, *4*(4), 300–304. https://doi.org/10.18178/joace.4.4.300-304
4. Gonzalez-Buelga, A., Clare, L.R., Neild, S.A., Burrow, S.G., & Inman, D.J. (2015). An electromagnetic vibration absorber with harvesting and tuning capabilities. *Structural Control and Health Monitoring*, *22*(11), 1359–1372. https://doi.org/10.1002/stc.1748
5. John, E.D. & Wagg, D.J. (2019). Design and testing of a frictionless mechanical inerter device using living-hinges. *Journal of the Franklin Institute*, *356*(14), 7650–7668. https://doi.org/10.1016/j.jfranklin.2019.01.036
6. Li, J.Y., Nie, Z.Y., Chen, Y.F., Ge, D.Q., & Li, M.Q. (2023). Development of boom posture adjustment and control system for wide spray boom. *Agriculture*, *13*(11), Article 2162. https://doi.org/10.3390/agriculture13112162
7. Li, Z.X., Cui, Z., & Li, M. (2014). Modeling of interlinked air suspension and study on its dynamic performance. *Applied Mechanics and Materials*, *494–495*, 163–166. https://doi.org/10.4028/www.scientific.net/AMM.494-495.163
8. Ma, R., Bi, K., & Hao, H. (2021). A novel rotational inertia damper for amplifying fluid resistance: Experiment and mechanical model. *Mechanical Systems and Signal Processing*, *149*, Article 107313. https://doi.org/10.1016/j.ymssp.2020.107313
9. Oda, N. & Nishimura, S. (1970). Vibration of air suspension bogies and their design. *Bulletin of JSME*, *13*(55), 43–50. https://doi.org/10.1299/jsme1958.13.43
10. Papageorgiou, C., Houghton, N.E., & Smith, M.C. (2009). Experimental testing and analysis of inerter devices. *Journal of Dynamic Systems, Measurement, and Control*, *131*(1), Article 011001. https://doi.org/10.1115/1.3023120
11. Quaglia, G. & Sorli, M. (2001). Air suspension dimensionless analysis and design procedure. *Vehicle System Dynamics*, *35*(6), 443–475. https://doi.org/10.1076/vesd.35.6.443.2040
12. Sammier, D., Sename, O., & Dugard, L. (2003). Skyhook and H8 control of semi-active suspensions: Some practical aspects. *Vehicle System Dynamics*, *39*(4), 279–308. https://doi.org/10.1076/vesd.39.4.279.14149

13. Seifi, A. & Hassannejad, R. (2022). Parameters uncertainty in pareto optimization of nonlinear inerter-based suspension system under nonstationary random road excitation. *Proceedings of the Institution of Mechanical Engineers, Part D: Journal of Automobile Engineering*, *236*(12), 2725–2744. https://doi.org/10.1177/09544070211060936

14. Shen, Y.J., Chen, A., Du, F., Yang, X.F., Liu, Y.L., & Chen, L. (2024a). Performance enhancements of semi-active vehicle air ISD suspension. *Proceedings of the Institution of Mechanical Engineers, Part D: Journal of Automobile Engineering*. https://doi.org/10.1177/09544070241233024

15. Shen, Y.J., Hua, J., Fan, W., Liu, Y.L., Yang, X.F., & Chen, L. (2023a). Optimal design and dynamic performance analysis of a fractional-order electrical network-based vehicle mechatronic ISD suspension. *Mechanical Systems and Signal Processing*, *184*, Article 109718. https://doi.org/10.1016/j.ymssp.2022.109718

16. Shen, Y.J., Jia, M.Q., Yang, X.F., Liu, Y.L., & Chen, L. (2023b). Vibration suppression using a mechatronic PDD-ISD-combined vehicle suspension system. *International Journal of Mechanical Sciences*, *250*, Article 108277. https://doi.org/10.1016/j.ijmecsci.2023.108277

17. Shen, Y.J., Qiu, D.D., Yang, X.F., Chen, J.J., Guo, Y., & Zhang, T.Y. (2024b). Vibration isolation performance analysis of a nonlinear fluid inerter-based hydro-pneumatic suspension. *International Journal of Structural Stability and Dynamics*. https://doi.org/10.1142/S0219455426500793

18. Smith, M.C. (2002). Synthesis of mechanical networks: the inerter. *IEEE Transactions on Automatic Control*, *47*(10), 1648–1662. https://doi.org/10.1109/TAC.2002.803532

19. Wang, F.C., Hong, M.F., & Lin, T.C. (2011). Designing and testing a hydraulic inerter. *Proceedings of the Institution of Mechanical Engineers, Part C: Journal of Mechanical Engineering Science*, *225*(1), 66–72. https://doi.org/10.1243/09544062JMES2199

20. Wang, Y., Wang, P., Meng, H., & Chen, L., (2024a). Dynamic performance and parameter optimization of a half-vehicle system coupled with an inerter-based X-structure nonlinear energy sink. *Applied Mathematics and Mechanics*, *45*(1), 85–110. https://doi.org/10.1007/s10483-024-3070-7

21. Wang, Y., Xu, B., & Meng, H. (2024b). Enhanced vehicle shimmy performance using inerter-based suppression mechanism. *Communications in Nonlinear Science and Numerical Simulation*, *130*, Article 107800. https://doi.org/10.1016/j.cnsns.2023.107800

22. Wen, G.L., Lei, Z.H., Yin, J.W., & Yin, H.F. (2013). Cushion characteristics of an omni-directional and multi-chamber airbag (in Chinese). *Journal of Vibration and Shock*, *32*(8), 13–17.

23. Yang, X., Zhang, T., Shen, Y., Liu, Y., Bui, V., & Qiu, D. (2024). Tradeoff analysis of the energy-harvesting vehicle suspension system employing inerter element. *Energy*, *308*, Article 132841. https://doi.org/10.1016/j.energy.2024.132841

Manuscript received February 29, 2024; accepted for publication January 8, 2025; published online March 22, 2025.